








Mapping and engineering of auxin-induced plasma membrane dissociation in BRX family proteins

Samuel W. H. Koh ¹, Petra Marhava ¹, Surbhi Rana ¹, Alina Graf ², Bernard Moret ¹,
Alkistis E. L. Bassukas ², Melina Zourelidou ², Martina Kolb ², Ulrich Z. Hammes ²,
Claus Schwechheimer ² and Christian S. Hardtke ^{1,*†}

¹ Department of Plant Molecular Biology, University of Lausanne, Biophore Building, Lausanne 1015, Switzerland

² Plant Systems Biology, Technical University of Munich, Freising 85354, Germany

*Author for correspondence: christian.hardtke@unil.ch

†Senior author.

The author responsible for distribution of materials integral to the findings presented in this article in accordance with the policy described in the Instructions for Authors (<https://academic.oup.com/plcell>) is: Christian S. Hardtke (christian.hardtke@unil.ch).

C.S.H., C.S., and U.Z.H. designed the research. S.W.H.K. performed most of the experiments. P.M., S.R., and B.M. performed some of the experiments. A.G., A.E.L.B., and M.Z. performed kinase assays. M.K. performed oocyte assays. All authors analyzed data and commented on the manuscript. S.W.H.K., C.S., and C.S.H. wrote the manuscript.

Abstract

Angiosperms have evolved the phloem for the long-distance transport of metabolites. The complex process of phloem development involves genes that only occur in vascular plant lineages. For example, in *Arabidopsis thaliana*, the *BREVIS RADIX* (*BRX*) gene is required for continuous root protophloem differentiation, together with *PROTEIN KINASE ASSOCIATED WITH BRX* (*PAX*). *BRX* and its *BRX-LIKE* (*BRXL*) homologs are composed of four highly conserved domains including the signature tandem *BRX* domains that are separated by variable spacers. Nevertheless, *BRX* family proteins have functionally diverged. For instance, *BRXL2* can only partially replace *BRX* in the root protophloem. This divergence is reflected in physiologically relevant differences in protein behavior, such as auxin-induced plasma membrane dissociation of *BRX*, which is not observed for *BRXL2*. Here we dissected the differential functions of *BRX* family proteins using a set of amino acid substitutions and domain swaps. Our data suggest that the plasma membrane-associated tandem *BRX* domains are both necessary and sufficient to convey the biological outputs of *BRX* function and therefore constitute an important regulatory entity. Moreover, *PAX* target phosphosites in the linker between the two *BRX* domains mediate the auxin-induced plasma membrane dissociation. Engineering these sites into *BRXL2* renders this modified protein auxin-responsive and thereby increases its biological activity in the root protophloem context.

Introduction

Angiosperms have evolved a vascular system that allows for the separation of the sites of water and nutrient acquisition from the sites of photosynthesis (Lucas et al., 2013). Shoot performance depends on water and inorganic nutrients delivered by the root system through the xylem, and in turn, root system growth depends on carbohydrates delivered by

the shoot through the phloem. More generally, the phloem connects source organs with sink organs and is, therefore, essential for sustained plant growth and development. Compared to other vascular tissues, the phloem is unique in its structure, function, and transport characteristics (Knoblauch et al., 2016). The phloem found in angiosperms consists of precisely aligned sieve elements, enucleated cells

that form the phloem sap-conducting sieve tubes, and their neighboring, supporting companion cells. Genes that are involved in the formation of phloem are typically specific to land plants. For example, *BREVIS RADIX* (*BRX*) and its homologs constitute small gene families in angiosperms (Briggs et al., 2006; Beuchat et al., 2010), but *BRX* homologs can already be found in mosses or lycophytes (One Thousand Plant Transcriptomes, 2019).

BRX was originally identified as the causative loss-of-function locus for the short root phenotype in the *Arabidopsis thaliana* stock center accession Umrkirch-1 (Mouchel et al., 2004). Research based on a null allele in the Col-0 reference accession confirmed requirement of *BRX* for primary root growth vigor (Rodrigues et al., 2009) and led to the realization that the causative cellular defect in *brx* mutants is their incapacity to form fully differentiated protophloem sieve element (PPSE) strands in the root meristem (Scacchi et al., 2010; Anne and Hardtke, 2017). Protophloem is early, meristematic phloem that is essential for root growth and maintenance (Furuta et al., 2014; Rodriguez-Villalon et al., 2014; Anne and Hardtke, 2017). Matching the location of the defect in *brx* mutants, the *BRX* protein is specifically expressed in developing protophloem, albeit at very low level (Bauby et al., 2007; Rodriguez-Villalon et al., 2014; Marhava et al., 2018).

The protophloem differentiation defects in *brx* mutants are not fully penetrant but rather occur in a nonrandom pattern, which has recently been explained by competition among neighboring sieve element precursors for auxin (Moret et al., 2020). Auxin flux through developing PPSE cell files controls the timing of their differentiation (Santuari et al., 2011; Marhava et al., 2018), and *BRX* has been implicated in regulating this polar auxin transport (Santuari et al., 2011; Marhava et al., 2018; 2020). *BRX* is a conditional plasma membrane-associated protein, which typically localizes to the rootward end of developing PPSEs. There it interacts and co-localizes with PROTEIN KINASE ASSOCIATED WITH *BRX* (*PAX*), a positive regulator of PIN-FORMED-1 (PIN)-mediated auxin efflux (Barbosa et al., 2018; Marhava et al., 2018). Because the plasma membrane association of *BRX* is negatively regulated by auxin and because *BRX* can interfere with PIN activation by *PAX* (Scacchi et al., 2009; Marhava et al., 2018), the three proteins are thought to constitute a molecular rheostat. In this model, inhibition of *PAX* by *BRX* suppresses PIN efflux activity, which in turn leads to increases in cytosolic auxin levels and thus the eventual dissociation of *BRX*, followed by *PAX* and PIN activation (Marhava et al., 2018). The ensuing dynamic equilibrium fine-tunes auxin flux through the developing protophloem.

The *A. thaliana* genome encodes five highly related *BRX* family proteins, which display four conserved domains that are separated by spacer regions: the N-terminus with a putative palmitoylation site (Rowe et al., 2019), an adjacent domain with a conserved “KDMA” motif, and two so-called “*BRX* domains” in tandem (Supplemental Figure S1A). Besides the *bona fide* *BRX* family genes, the *A. thaliana*

genome contains another partial *BRX* homolog (AT2G21030), which encodes a nearly identical but incomplete first *BRX* domain, the linker, and part of the second *BRX* domain, whereas the N-terminal parts of *BRX* are missing (Supplemental Figure S1B). Ectopic expression and promoter-swapping experiments suggested that only the closest *BRX* homolog, *BRX-LIKE1* (*BRXL1*), can fully substitute for *BRX*, whereas *BRXL2*–*BRXL4* at best confer partial rescue of *brx* mutants (Briggs et al., 2006; Beuchat et al., 2010). In contrast to *BRX*, the plasma membrane association of *BRXL2* is not auxin-responsive, and its capacity to inhibit *PAX* is reduced (Marhava et al., 2020). These differential features may be responsible for the incapacity of *BRXL2* to fully substitute for *BRX* function, as other protein–protein interaction properties and polar, rootward plasma membrane association are shared (Marhava et al., 2020). However, *BRX* and *BRXL2* are fully redundant in the context of stomata development, where *BRXL2* is the dominant family member (Bringmann and Bergmann, 2017; Rowe et al., 2019). Here, we embarked on a detailed comparative analysis of *BRX* family protein domains to further our understanding of this interesting class of land plant-specific proteins. Our data suggest that the auxin response of *BRX* is conferred by the linker region between the tandem *BRX* domains and by *PAX* kinase target phosphosites. Engineering these sites into *BRXL2* renders the protein auxin-responsive and increases its biological activity in the root protophloem.

Results

Expression level and auxin response determine redundancy among *BRX* family proteins

The defect in *A. thaliana* *brx* root meristems manifests itself in developing PPSE strands that are interrupted by PPSE precursors that do not properly differentiate, i.e. so-called gap cells. Gap cell frequency in one or both PPSE strands is one of the quantitative readouts of phenotypic severity in pertinent mutants (Breda et al., 2017). Typically, ~50%–60% of *brx* root meristems show gap cells in one PPSE strand, whereas ~20%–30% show gap cells in both strands (Supplemental Figure S2A). In available *brx brxl1 brxl2 brxl3* quadruple mutants (Rowe et al., 2019), this defect tended to be enhanced relative to *brx* single mutants (Supplemental Figure S2A), and in extremis, PPSE differentiation was nearly absent (Supplemental Figure S2B). The enhanced severity of the quadruple mutant also manifested itself in eventually even further reduced root growth compared to the *brx* single mutant (Supplemental Figure S2C). In contrast, knockout of the partial *BRX* homolog AT2G21030, whose promoter is active in the mature root vasculature but not in developing protophloem (Supplemental Figure S2D), did not result in any detectable root development defects (Supplemental Figure S1B). These results suggest limited yet tangible redundancy between *BRX* and other *BRX* family genes in the root.

Previous work suggested that the closest *BRX* homolog, *BRXL1*, is mainly expressed in the mature vasculature (Scacchi et al., 2009; Cattaneo et al., 2019). However, some

weak expression and rootward polar localization in the protophloem was observed when a BRXL1–CITRINE fusion protein was expressed in the genomic *BRXL1* context (Figure 1A). In contrast, BRXL2–CITRINE fusion protein expressed in the genomic *BRXL2* context was observed throughout the root and also displayed rootward polarity (Marhava et al., 2020), which was accentuated in developing protophloem (Figure 1B). Interestingly, BRXL2–CITRINE expression was also observed in the stem cell niche and in the columella-root cap. Although the *BRX* promoter confers expression in these tissues as well (Scacchi et al., 2009) (Supplemental Figure S2E), BRX protein is barely detectable there (Marhava et al., 2018). The latter might reflect destabilization of BRX by auxin (Supplemental Figure S2F), which accumulates in and around the stem cell niche (Sabatini et al., 1999; Grieneisen et al., 2007).

When expressed in a *brx* background, increased *BRXL1* dosage through *BRXL1:gBRXL1-CITRINE* transgene expression conferred partial rescue of the *brx* mutant phenotype (Figure 1, C and D), and this rescue was quantitatively comparable to the partial rescue conferred by expression of the *BRXL2:gBRXL2-CITRINE* transgene in *brx* (Figure 1, E and F). However, *brx* rescue was nearly perfect when BRXL1–CITRINE was expressed under the control of the *BRX* promoter (Figure 1, G–I), but not when BRXL2–CITRINE was expressed in the same context (see below) (Marhava et al., 2020). Moreover, similar to BRX–CITRINE (Figure 1J), the plasma membrane association and stability of BRXL1–CITRINE were auxin-responsive (Figure 1, K and L), in stark contrast to BRXL2–CITRINE (Marhava et al., 2020) (Figure 1M). In summary, these observations support the notion that the auxin-responsiveness of BRX is critical for its regulatory function in protophloem development and that the closely related BRXL1, but not the divergent BRXL2, shares this functionally important property. Furthermore, the strong functional overlap between BRX and BRXL1 proteins is only set aside by divergent expression levels, with the *BRX* promoter conferring substantially higher expression than the *BRXL1* promoter.

Plasma membrane association is a robust feature of BRX function

To better understand putative BRX functional domains, we explored sequence features that could be related to BRX localization, stability, or turnover (Supplemental Figure S3). First, we targeted the N-terminal amino acids, which confer robust plasma membrane association in the case of BRX (Scacchi et al., 2009) and contain a putative palmitoylation site (Rowe et al., 2019). Interestingly, BRX and BRXL1 differ at amino acid 2 (phenylalanine) from the other family members (leucine). Because BRX might be targeted by the ubiquitin–proteasome pathway (Scacchi et al., 2009), we replaced the destabilizing N-end rule phenylalanine residue by methionine (BRX^{F2M}). However, this BRX^{F2M} version did not display any substantially different stability compared to wild-type BRX (Figure 2, A and B). Next, we added a

myristoylation signal to the N-terminus (BRX^{N-MYR}) (Bologna et al., 2004) and compared it to a control protein with a similar sized added random sequence (BRX^{N-EXT}). Again, no substantially different localization was observed (Figure 2, C and D), except that the plasma membrane association of BRX^{N-MYR} appeared somewhat “cleaner.” Interestingly, the myristoylation signal neither interfered with BRX polarity nor with its auxin response (Figure 2, E and F). This matches the idea that auxin-induced BRX dissociation from the plasma membrane could involve clathrin-mediated endocytosis (Scacchi et al., 2009; Santuari et al., 2011). Finally, we revisited the potential nuclear localization requirement of BRX (Scacchi et al., 2009) by either mutating its nuclear exclusion signal (BRX^{NES > mut}), replacing it with a nuclear localization signal (BRX^{NES > NLS}), or adding an artificial nuclear localization signal to the C-terminus (BRX^{C-NLS}). Whereas the BRX^{NES > mut} protein appeared somewhat stabilized (Supplemental Figure S4A), the BRX^{NES > NLS} and BRX^{C-NLS} proteins appeared to be less abundant than wild-type BRX (Supplemental Figure S4, B and C). Yet remarkably, both BRX^{NES > NLS} and BRX^{C-NLS} were predominantly plasma membrane associated and were barely visible in the nucleus, suggesting that the presence of a nuclear localization signal could not override its plasma membrane association. Despite these slightly divergent behaviors of different BRX variant proteins, all of them fully rescued the root growth defect of *brx* (Supplemental Figure S4D), and no protophloem gaps were observed in these lines. In summary, none of our amino acid exchanges or additions had a major impact on the plasma membrane association of BRX or the capacity to rescue the signature defects of the *brx* mutant.

The tandem BRX domains comprise the essential features of BRX activity

To delimit functionally relevant domains of BRX, we expressed deletion constructs in the *brx* mutant background. To this end, the potentially palmitoylated BRX N-terminus (Rowe et al., 2019) (amino acids 1–9) was combined with different BRX subfragments that were designed to encompass the different conserved domains (Supplemental Figure S1A). These fragments were expressed as CITRINE fusions under the control of the *BRX* promoter. All five fragments tested showed plasma membrane association and expression in PPSEs (Figure 3, A–E). Yet, the fragments that contained no or only one BRX domain displayed more variable plasma membrane localization and at times expression outside of the PPSE strands (Figure 3, A–C). This also matched expression pattern of a nuclear localized NLS–VENUS fusion protein under the control of the full-length *BRX* promoter or its rather extended 2,314 bp 5′-UTR only (Figure 3, F and G). In contrast, the fragment that comprised both BRX domains (BRX^{104–344}) invariably and precisely mimicked the plasma membrane localization and expression pattern of full-length BRX (Figure 3D). This highly PPSE-specific expression was also consistent with the striking, serendipitous observation that expression of the full-length

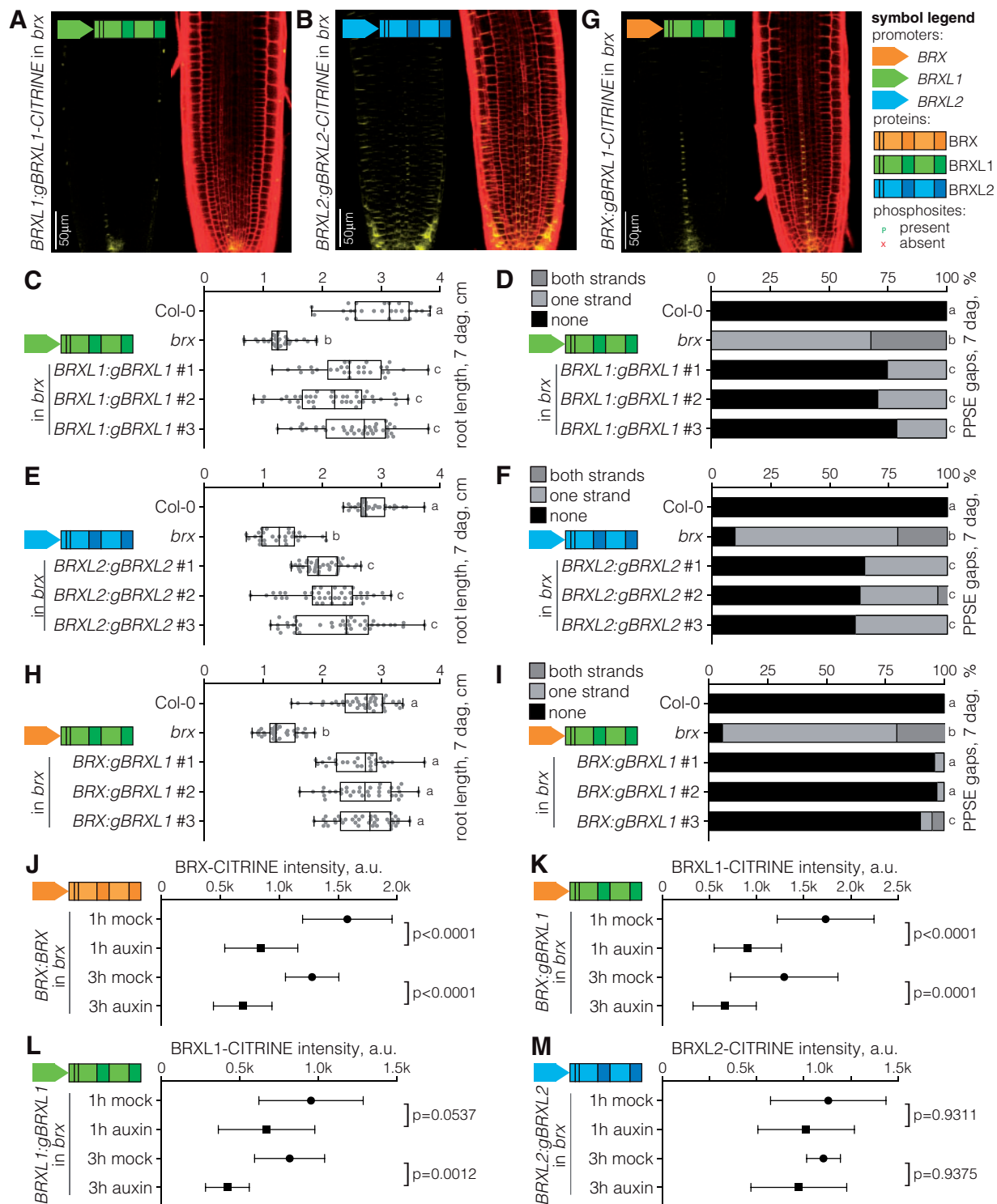


Figure 1 Limited redundancy of *BRX* family genes in the root protophloem. The symbol legend shows schematic overviews of the *BRX* gene family constructs used in this and subsequent figures. A, Confocal microscopy image of BRXL1–CITRINE fusion protein fluorescence expressed in the genomic *BRXL1* context in the *brx* mutant background (yellow fluorescence, left), and overlaid with PI-stained cell wall outline (red fluorescence, right). B and G, As in (A), for *BRXL2* (B) or *BRXL1* expressed under the control of the *BRX* promoter (G). C, E, and H, Root length of Col-0 wild-type, *brx* mutant, and the indicated transgenic lines (three representative independent lines, $n = 26–43$ roots). Transgenic proteins were expressed in fusion with C-terminal CITRINE tags. Box plots display second and third quartiles and the median, bars indicate maximum and minimum. Statistical significance was determined by ordinary one-way ANOVA. dag, days after germination. D, F, and I, PPSE strand defects in the roots of the indicated genotypes, expressed as the frequency of root meristems with nondifferentiating “gap cells” in both, one, or none of the developing PPSE strands ($n = 27–51$ roots). Statistical significance was determined by Fisher’s exact test. J–M, Quantification of the indicated CITRINE fusion protein signal intensity at the rootward plasma membrane of developing PPSEs, 1 or 3 h after mock (DMSO) or auxin ($10 \mu\text{M}$ 1-naphthalene-acetic acid) treatment ($n = 8–23$ roots, average of 12–15 cells per root). Plot circles and squares display the mean, error bars indicate standard deviation. Statistical significance was determined by ordinary one-way ANOVA. a.u., arbitrary units. Statistically significant different groups are indicated by different lowercase letters.

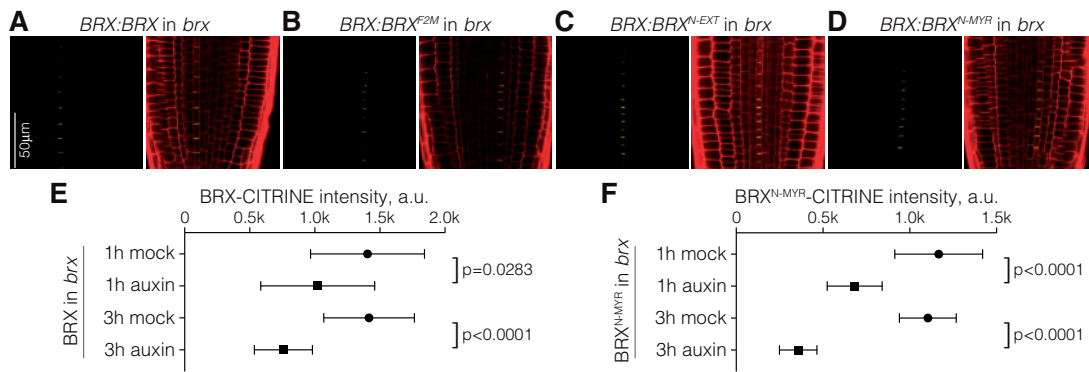


Figure 2 Robust plasma membrane association of BRX N-terminal variants. A–D, Confocal microscopy images of variant BRX–CITRINE fusion proteins (see Supplemental Figure S3) expressed under the control of the *BRX* promoter in the *brx* mutant background (yellow fluorescence, left). (Right) Overlay with PI cell wall staining (red fluorescence). E and F, Quantification of the indicated CITRINE fusion protein signal intensity at the rootward plasma membrane of developing PPSEs, 1 or 3 h after mock or auxin treatment ($n = 12–23$ roots, average of 12–15 cells per root). Plot circles and squares display the mean, error bars indicate standard deviation. Statistical significance was determined by ordinary one-way ANOVA.

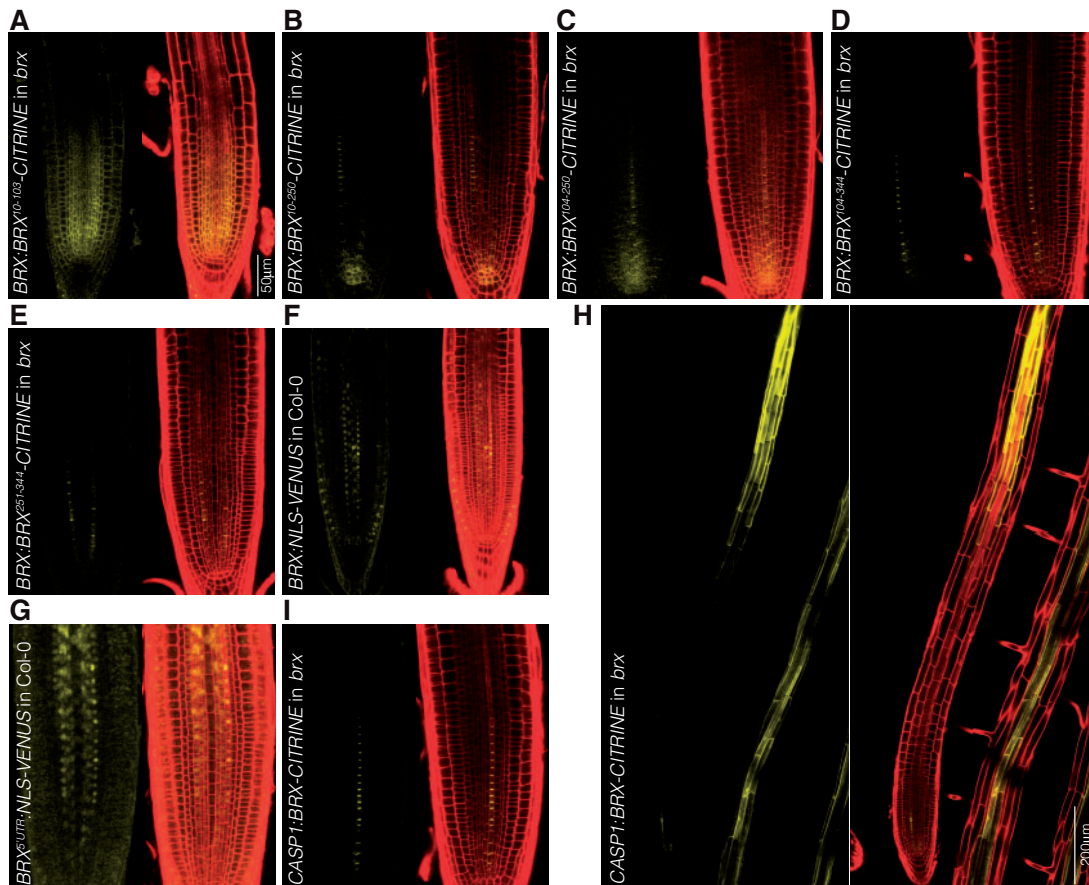


Figure 3 The *BRX* transcript sequence confers expression in the root protophloem. A–E, Confocal microscopy images of BRX protein fragments fused with CITRINE tags (yellow fluorescence, left), expressed under the control of the *BRX* promoter in the *brx* mutant background. (Right) Overlay with PI cell wall staining (red fluorescence). Superscripts indicate the amino acid fragments. Note that all fragments were preceded by amino acids 1–9. F and G, Confocal microscopy images of NLS–VENUS fusion protein expressed in Col-0 under the control of the full-length *BRX* promoter (F) or the 5′-UTR only (G). H and I, Confocal microscopy images of full-length BRX–CITRINE fusion protein expressed in *brx* under the control of the *CASP1* promoter, illustrating expression in the late endodermis (H) but also the protophloem (I).

BRX coding sequence under the control of ectopic promoters, such as the late endodermis-specific *CASPARIAN STRIP MEMBRANE DOMAIN PROTEIN1* (*CASP1*) promoter

(Roppolo et al., 2011), fully rescued the *brx* root phenotype (Supplemental Figure S5, A and B) and conferred BRX–CITRINE expression in PPSEs, outside the *CASP1* domain (Figure 3, H

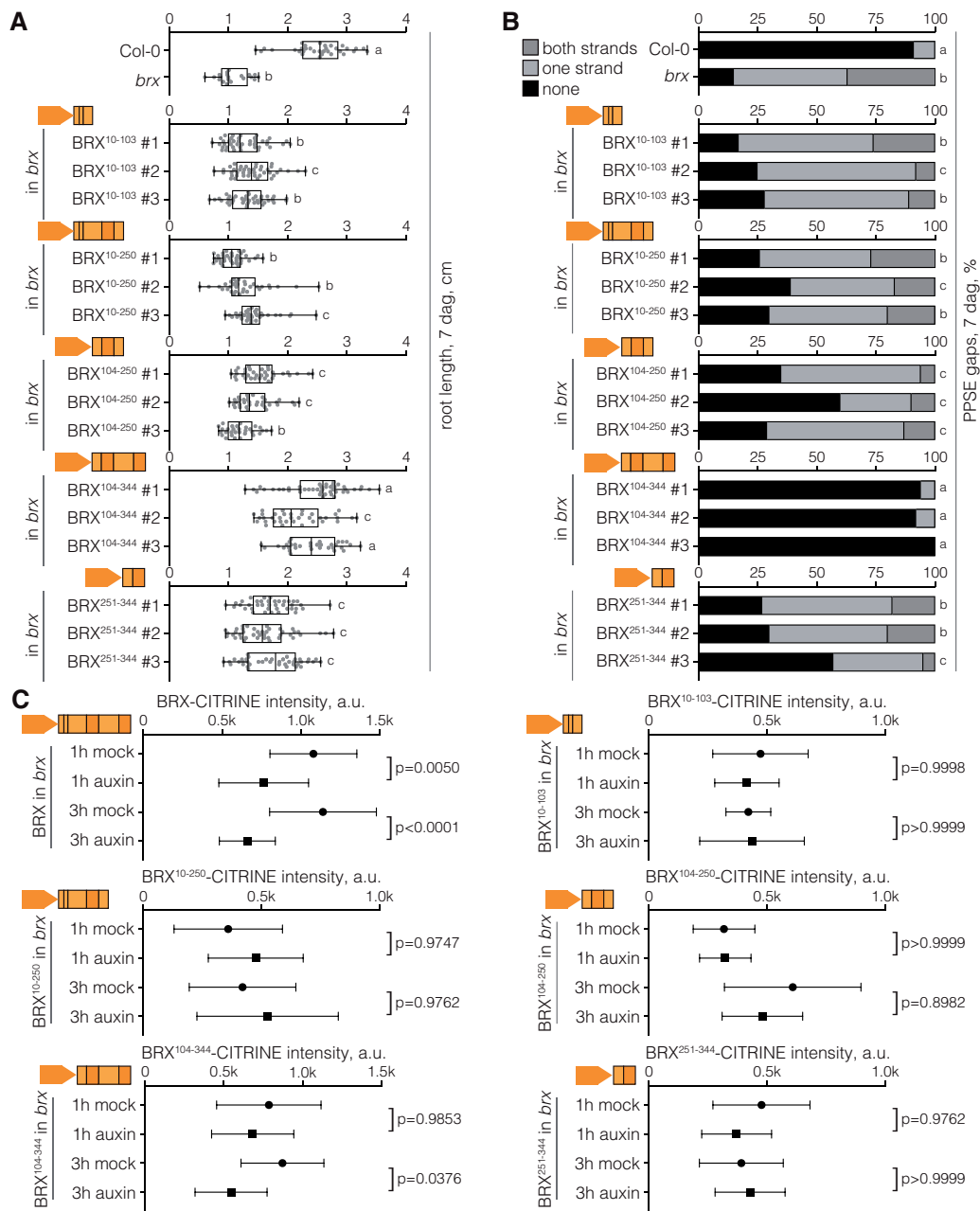


Figure 4 The tandem BRX domains are necessary and sufficient for BRX function in the protophloem. **A**, Root length of Col-0, *brx*, and plants harboring the indicated transgenic BRX fragments (three representative independent lines, $n = 20-45$ roots). Superscripts indicate the amino acid fragments. Note that all fragments were preceded by amino acids 1-9 and fused to C-terminal CITRINE tags. Box plots display second and third quartiles and the median, bars indicate maximum and minimum. Statistical significance was determined by ordinary one-way ANOVA. **B**, PPSE strand defects in roots of the indicated genotypes ($n = 15-24$), corresponding to (A). Statistical significance was determined by Fisher's exact test. **C**, Quantification of the indicated CITRINE fusion protein signal intensity at the rootward plasma membrane of developing PPSEs, 1 or 3 h after mock or auxin treatment ($n = 10-23$ roots, average of 12-15 cells per root). Plot circles and squares display the mean, error bars indicate standard deviation. Statistical significance was determined by ordinary one-way ANOVA. Statistically significant different groups are indicated by different lowercase letters.

and I). Collectively, these observations suggest that the coding region encompassing the BRX domains is a major determinant for the PPSE-specific BRX expression pattern.

At the level of biological function, the BRX¹⁰⁴⁻³⁴⁴ fragment was also the only one that nearly perfectly normalized both the root growth and protophloem differentiation defects of

brx mutants (Figure 4, A and B). Moreover, it was also the only fragment whose plasma membrane association displayed a statistically significant response to auxin treatment (Figure 4C). In summary, our experiments suggest that, together with the short, conserved N-terminus, the fragment comprising the tandem BRX domains is sufficient to convey

the biological outputs of BRX function that are captured by our assays.

The linker between the BRX domains functionally differentiates BRX family proteins

Next, we sought to map the differential plasma membrane association in response to auxin in BRX and BRXL2. To this end, we created a number of hybrids between the two proteins (Supplemental Figure S6). In each case, expression of these BRX–BRXL2 hybrids as CITRINE fusion proteins under the control of the BRX promoter in the *brx* background displayed the PPSE-specific pattern observed for wild-type BRX (Figure 5, A–D). However, the hybrid proteins differed in their capacity to normalize the protophloem and root growth defects of *brx* (Figure 5, E–L). Essentially, the capacity for complementation gradually increased as the portion of BRX extended from the N-terminus, and only the hybrid that combined the BRX N-terminal fragment including the first BRX domain with the second, C-terminal BRX domain of BRXL2 (BRX^{HYB250|254}) was able to largely (although not perfectly) rescue the hallmark *brx* phenotypes (Figure 5, H and L). Matching these observations, the hybrids with a larger portion of BRXL2 did not display a significant auxin response (Figure 6, A–C), whereas the BRX^{HYB250|254} hybrid was as auxin-responsive as wild-type BRX (Figure 6D). These results suggest that the sequence determinants for the auxin-responsive plasma membrane dissociation of BRX reside between amino acids 138 and 250, that is within, or close to, the first of the two BRX domains.

Sequence alignment pointed toward a potential role for the linker between the tandem BRX domains, because it is clearly different between BRX and BRXL1 on the one side and BRXL2–BRXL4 on the other (Supplemental Figure S1A; Figure 7A). Interestingly, the portion of the BRX linker that was present in BRX^{HYB250|254}, encompassing amino acids 197–250, contained two R(D/E)S motifs that are also conserved in BRXL1 but absent from other BRX family proteins (Supplemental Figure S1A). These motifs, as well as another BRX/BRXL1-specific RES site before the first BRX domain (Figure 7A), could constitute potential target sites for AGC kinases such as D6 PROTEIN KINASE (D6PK) or PAX (Huang et al., 2010; Zourelidou et al., 2014). Indeed, in replicate in vitro kinase assays with recombinant GST–BRX fusion protein and phosphosite-mutant variants including S (serine) to A (alanine) substitutions of the pertinent serines 123, 217, and 228, the S228A mutation led to the strongest reduction in BRX phosphorylation by D6PK as well as by PAX compared to BRX wild-type protein phosphorylation (Figure 7, B and C). Finally, in phospho-proteomics replicates of BRX–CITRINE fusion protein that was immuno-purified from VISUAL assays (Kondo et al., 2016; Marhava et al., 2018), S228 was identified as a high confidence in vivo phosphosite (Figure 7A). In contrast, these data did not provide evidence for phosphorylation on S123, and S217 was not covered in these analyses. Although the intersection of our various assays points to a key role for the S228 phosphosite,

at this point, we cannot exclude the possibility that the other phosphosites do not at least contribute to the response. Nevertheless, together, these experiments suggest that the linker between the tandem BRX domains, which includes S228, has a crucial function in the differential activity of BRX and BRXL2 and that phosphosites targeted by PAX or D6PK might have a role in this differentiation.

Engineered phosphosites are sufficient to impart an auxin response to a BRX family protein

To assess the functional significance of these findings *in planta*, we investigated a BRX variant in which the three serines in the potential D6PK/PAX R(D/E)S target sites (S123, S217, and S228) were substituted by alanines (BRX^{3PKO}) (Supplemental Figure S7). Expression and localization of BRX^{3PKO}–CITRINE fusion protein appeared normal (Supplemental Figure S8A) and largely rescued the protophloem and root growth phenotypes of *brx* (Figure 8A). However, compared to the rescue obtained with wild-type BRX (Figure 8B), the rescue was never perfect. Even in the best-complemented lines, some level of PPSE defect persisted, and root growth rescue was highly variable (Figure 8, C and D). Most importantly, plasma membrane-associated BRX^{3PKO} no longer displayed a significant auxin response (Figure 8, E and F), but BRX^{3PKO} was still about as efficient as wild-type BRX in inhibiting D6PK-stimulated auxin efflux in *Xenopus laevis* oocyte assays (Supplemental Figure S8B). Together, these data suggest that PAX- and D6PK-targeted phosphosites contribute to the fine-tuning of BRX function and modulate its auxin-responsiveness.

To independently verify this finding, we investigated a BRX homolog from a descendant of the most ancient vascular plant lineage, the lycophyte *Selaginella moellendorffii*. As far as we could determine, the *S. moellendorffii* genome (Banks et al., 2011) contains a single BRX homolog (*SmBRX*). The encoded protein already possesses all the highly conserved domains found in *A. thaliana* BRX family proteins, but the linker between the two BRX domains is by comparison very short and does not contain any putative D6PK or PAX target phosphosites (Figure 9A). Expression of an *A. thaliana* codon-optimized version of *SmBRX* as a CITRINE fusion under the control of the BRX promoter in the *brx* background recapitulated the *A. thaliana* BRX PPSE-specific expression pattern and protein localization (Supplemental Figure S8C). However, similar to BRX^{3PKO}, *SmBRX* did not fully rescue the *brx* mutant phenotypes (Figure 9, B and C), corroborating the importance of the linker and phosphosites for BRX function. Finally, as would be predicted from our previous observations, *SmBRX* protein was also not significantly auxin-responsive (Figure 9, D and E).

Because the lack of auxin-responsive plasma membrane dissociation was pinpointed as one of the factors that differentiate BRXL2 from BRX (Marhava et al., 2020), we modified BRXL2 by adding three putative D6PK/PAX target phosphosites at the positions corresponding to S123, S217, and S228 in BRX (BRXL2^{3PADD}) (Supplemental Figure S7). This

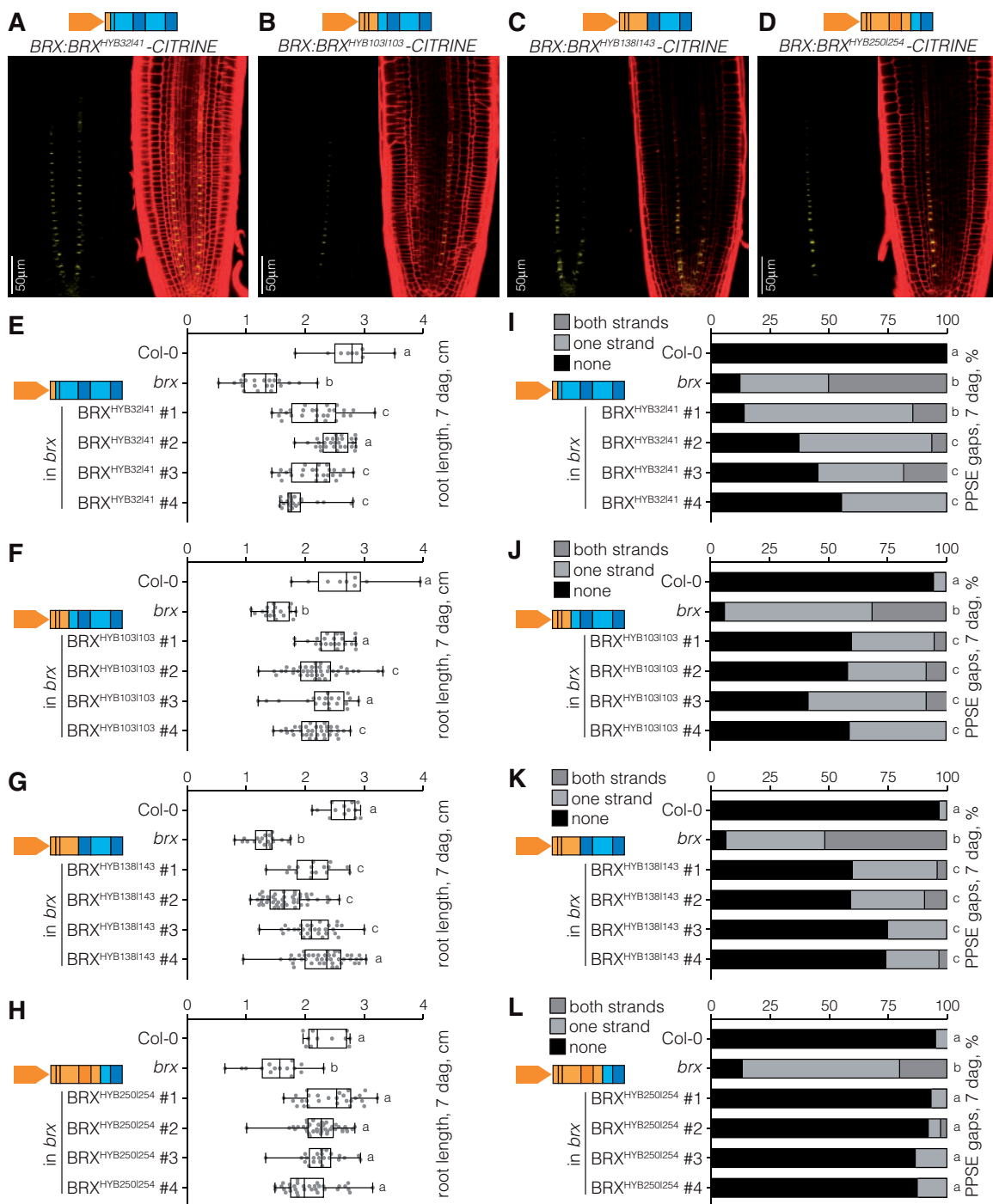


Figure 5 Differential activity of BRX versus BRXL2 residues in the tandem BRX domains. A–D, Confocal microscopy images of BRX–BRXL2 hybrid fusion proteins, tagged with CITRINE and expressed under the control of the *BRX* promoter in the *brx* mutant background (yellow fluorescence, left). Right: overlay with PI cell wall staining (red fluorescence). Superscripts indicate the last amino acid in the BRX portion and the first amino acid in the BRXL2 portion. E–H, Root length of Col-0, *brx*, and the indicated transgenic lines corresponding to (A–D) (four representative independent lines, $n = 10\text{--}48$ roots). Box plots display second and third quartiles and the median, bars indicate maximum and minimum. Statistical significance was determined by ordinary one-way ANOVA. I–L, PPSE strand defects in the roots of the indicated genotypes, corresponding to (E–H) ($n = 15\text{--}38$ roots). Statistical significance was determined by Fisher’s exact test. Statistically significant different groups are indicated by different lowercase letters.

BRXL2^{3PADD}-CITRINE fusion protein displayed PPSE-specific expression and polar, rootward plasma membrane association when expressed under the control of the *BRX* promoter in the *brx* background (Supplemental Figure S8D).

Moreover, this fusion protein partially rescued the proto-phloem and root growth defects of *brx* (Figure 10, A and B), and this rescue appeared to be substantially better than the partial rescue observed with BRXL2 wild-type protein

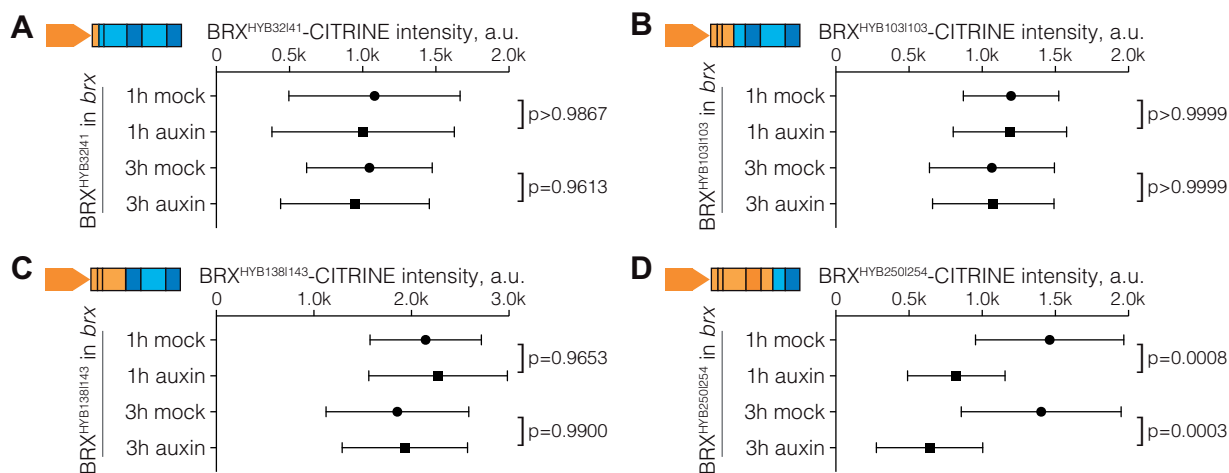


Figure 6 Mapping of the BRX auxin response using BRX–BRXL2 hybrid fusion proteins. A–D, Quantification of the indicated BRX–BRXL2 hybrid CITRINE fusion protein signal intensity at the rootward plasma membrane of developing PPSEs, 1 or 3 h after mock or auxin treatment ($n = 10$ – 18 roots, average of 12–15 cells per root). Plot circles and squares display the mean, error bars indicate standard deviation. Statistical significance was determined by ordinary one-way ANOVA.

(Marhava et al., 2020). Indeed, in direct comparisons, *brx* rescue was consistently more efficient with BRXL2^{3PADDD} than with BRXL2 wild-type protein (Figure 10, C and D). Finally, and most strikingly, unlike BRXL2 wild-type protein (Figure 10E), the plasma membrane association of BRXL2^{3PADDD} was sensitive to auxin treatment (Figure 10, F and G), at about the same magnitude as BRX (Figure 8E). These observations suggest that the addition of the three putative D6PK/PAX phosphosites is sufficient to impart an auxin response on BRXL2 and thereby increase its biological activity in the context of protophloem development.

Discussion

Recent work established that during protophloem development, BRX primarily acts as a switch element in conjunction with PAX to fine-tune auxin flux through developing PPSE strands (Marhava et al., 2018, 2020). In this study, we mapped functionally important regions of BRX and found that the plasma membrane-associated tandem BRX domains and their linker are sufficient to convey BRX action in the protophloem. This linker includes critical phosphosites that mediate the BRX auxin response and can impart this response on a modified BRXL2 protein. The modified, auxin-responsive BRXL2 displays increased functionality in PPSE development, where native, auxin-insensitive BRXL2 can only partially replace BRX (Briggs et al., 2006; Beuchat et al., 2010; Marhava et al., 2020). Our data thus suggest that among the *A. thaliana* BRX family proteins, BRX and its close homolog BRXL1 are uniquely suited to transmit both a PPSE-specific on-off signal through their regulated plasma membrane association and directional information through their asymmetric distribution. Only the latter part of this dual role seems to be required in the stomata context, where BRX can replace BRXL2 (Rowe et al., 2019). Our results also reiterate that auxin-responsive plasma

membrane dissociation is one of the features that quantitatively determine BRX activity in the protophloem context.

Intragenic BRX sequences contribute to its root protophloem-specific expression

An unexpected finding in our study was that the plasma membrane-associated tandem BRX domains and their linker are not only sufficient to convey BRX protein function in the root protophloem, but apparently also confer its highly PPSE-specific expression. Such contribution of intragenic sequences to gene expression patterns has been reported repeatedly (Sieburth and Meyerowitz, 1997; Cattaneo et al., 2019) and reiterates the finding that reporters of promoter activity do not always capture the exact expression domain. Notably, in the case of BRX, the genuine expression pattern has been verified by anti-BRX immunostaining (Marhava et al., 2018). Thus, it appears that the *BRX* promoter and intragenic sequences have co-evolved to synergistically confer highly PPSE-specific expression in the root meristem. The finding that BRXL1 can only fully substitute for BRX when expressed under the control of the *BRX* promoter supports this idea. Future comparative studies between *BRX* family genes as well as codon-optimized *BRX* versions might be able to pinpoint the key regulatory sequences and determine their relative contributions. In summary, our results suggest that the tandem BRX domains constitute a module that is intimately associated with protophloem differentiation on several regulatory levels.

BRX acts primarily at the plasma membrane

Interestingly, it has been demonstrated that mutation of cysteines 4 and 7 compromises the plasma membrane association of BRX and its function in stomata (Rowe et al., 2019). It was thus suggested that the BRX N-terminus could be reversibly palmitoylated, and that the auxin-induced plasma membrane dissociation of BRX might involve

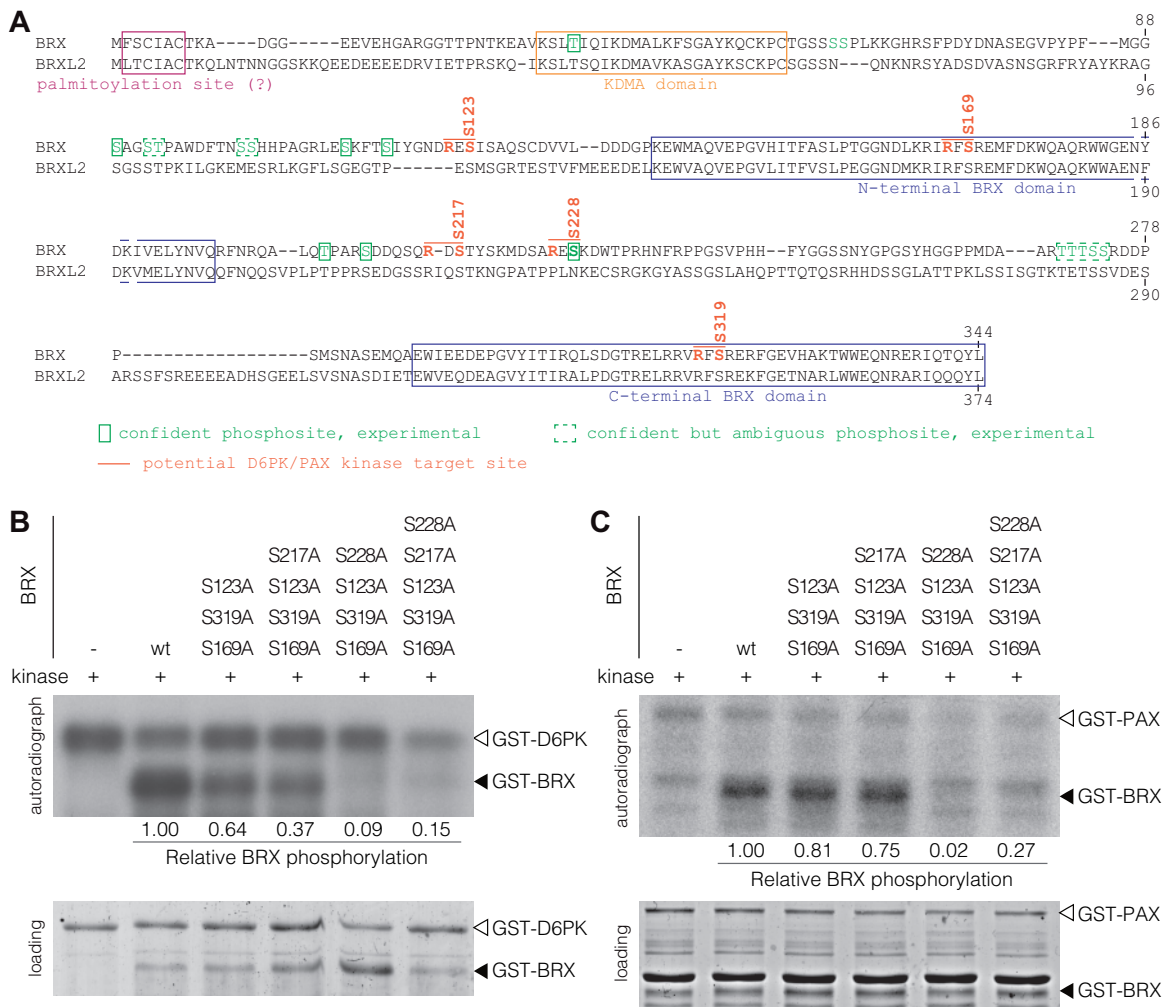


Figure 7 D6PK/PAX phosphosites in BRX. A, Amino acid sequence alignment of BRX and BRXL2, highlighting key features and phosphosites identified by proteomics in BRX. The R(D/E)S D6PK/PAX target site motifs present in BRX and BRXL1, but not in BRXL2–BRXL4, are highlighted. B and C, Representative results of in vitro kinase assays with bacterially expressed GST fusions of BRX wild-type protein and point mutant variants with the indicated (multiplexed) serine to alanine substitutions as the substrate, and a GST fusion of D6PK (B) or PAX (C) as the kinase. Substitutions of S123, S169, S217, S228, and S319 are in hypothetical D6PK/PAX target sites where the phosphosite serine is preceded by a variable residue and an arginine. The relative phosphorylation strength (as determined by density measurements) is specified below the autoradiograph. Please note that identical amounts of BRX were loaded in the PAX and D6PK reactions but that, in the PAX reactions, BRX loading is covered by a GST-PAX degradation product.

de-palmitoylation. Yet, the addition of myristoylation signals neither affected the intracellular polarity (Rowe et al., 2019) nor auxin-response of BRX. Because myristoylation is an irreversible post-translational modification, BRX internalization could reflect proteolytic removal of the N-terminus. Alternatively, the turnover of plasma membrane-localized BRX might involve clathrin-mediated endocytosis (Scacchi et al., 2009; Santuari et al., 2011), for which the rootward plasma membrane domain of PPSEs is a hotspot (Dettmer et al., 2014; Marhava et al., 2020).

BRX is an auxin-responsive plasma membrane-localized regulator of protophloem development. Our domain analyses suggest that the plasma membrane-associated tandem BRX domains (amino acids 1–9 plus 139–344) are sufficient to convey the biological functions of BRX that are captured in our phenotypic assays. Substantial but still partial rescue

of *brx* by the tandem BRX domains has been reported before (Scacchi et al., 2009). However, in those experiments, the fragment was constitutively over-expressed under the control of the 35S cauliflower mosaic virus promoter, and the BRX N-terminal amino acids 1–9 added in this study were missing. Because the (ectopically) over-expressed fragment showed relatively little plasma membrane association and, instead, was mostly found in the nucleus, this was taken as evidence that BRX has a function in the nucleus. This notion was supported by the observation that BRX could interact with transcription factors (Scacchi et al., 2009; 2010), accumulated in the nucleus when transiently expressed in onion (*Allium cepa*) epidermal cells, and stimulated transcription in yeast (Mouchel et al., 2004). Our findings are not in conflict with these earlier observations, but they diminish the functional importance of the nuclear

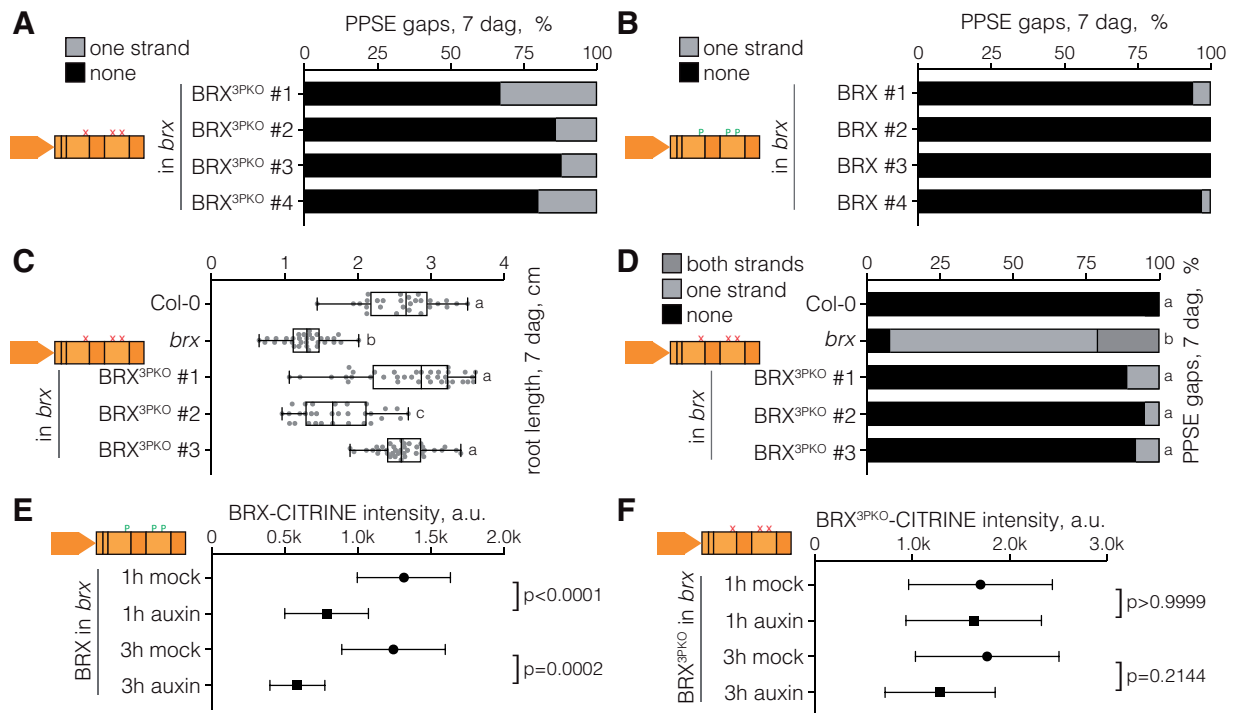


Figure 8 Amino acid substitutions in putative PAX phosphosites diminish BRX activity. A and B, PPSE strand defects in the roots of the indicated genotypes (four representative independent lines, $n = 13$ –20 roots). BRX^{3PKO} (B) carries three alanine substitutions for serines 123, 217, and 228. C, Root length of Col-0, *brx*, and three “best” BRX^{3PKO} independent transgenic lines ($n = 28$ –38 roots). Box plots display second and third quartiles and the median, bars indicate maximum and minimum. Statistical significance was determined by ordinary one-way ANOVA. D, PPSE strand defects in the roots of the indicated genotypes, corresponding to the samples scored in (C) ($n = 37$ –42 roots). Statistical significance was determined by Fisher’s exact test. E and F, Quantification of the indicated CITRINE fusion protein signal intensity at the rootward plasma membrane of developing PPSEs, 1 or 3 h after mock or auxin treatment ($n = 15$ –20 roots, average of 12–15 cells per root). Plot circles and squares display the mean, error bars indicate standard deviation. Statistical significance was determined by ordinary one-way ANOVA. Statistically significant different groups are indicated by different lowercase letters.

localization of BRX with regard to its known phloem functions. We found that BRX variants expressed in the root protophloem in the native context always display substantial plasma membrane association and are barely visible in the nucleus, even when explicitly targeted to the nucleus. Such variants are also still able to rescue the *brx* root growth and protophloem phenotypes. Our findings, therefore, suggest that, for now, no biological role can be firmly associated with the nuclear localization of BRX and that its previously proposed central function as a transcriptional regulator (Mouchel et al., 2004; Scacchi et al., 2009) has to be revised. Our data also resonate with the role of BRX in stomata formation, which requires the plasma membrane association of BRX, but not its nuclear localization (Rowe et al., 2019).

Phosphosites in the linker contribute to the functional divergence of BRX family proteins

Besides the possible role of post-translational modifications, the plasma membrane association of BRX in the protophloem largely depends on PAX, presumably by a direct protein–protein interaction (Marhava et al., 2018, 2020). Interestingly, the plasma membrane association of PAX is not sensitive to auxin, but auxin stimulates its kinase activity (Marhava et al., 2018). The latter may be conferred by recently identified, functionally

redundant upstream regulators of D6PK and PAX, the 3-PHOSPHOINOSITIDE-DEPENDENT PROTEIN KINASES (PDK1) and PDK2 (Zegzouti et al., 2006; Tan et al., 2020; Xiao and Offringa, 2020). It is, therefore, tempting to speculate that BRX turnover and dissociation from the plasma membrane are modulated by PAX-mediated phosphorylation. PAX activation by auxin and, therefore, the stimulation of PIN-mediated auxin efflux would thus be amplified by simultaneous removal of the PAX inhibitor BRX. A direct test of this conceptually attractive model through experimental means is unfortunately currently out of reach. Yet, our striking observation that engineering of putative D6PK/PAX target phosphosites into BRXL2, which can also interact with PAX (Marhava et al., 2020), renders the modified protein auxin-responsive supports this model. The finding that this modification also augments the activity of BRXL2 in the context of root protophloem development, whereas, conversely, loss of the corresponding phosphosites diminishes the auxin response and activity of BRX, further corroborates the quantifiable contribution of the auxin-induced plasma membrane dissociation of BRX to integrated PPSE differentiation and the rheostat model (Marhava et al., 2018).

Finally, our results also suggest that the functional divergence within the BRX protein family resides mainly in the linker between the tandem BRX domains. The tandem

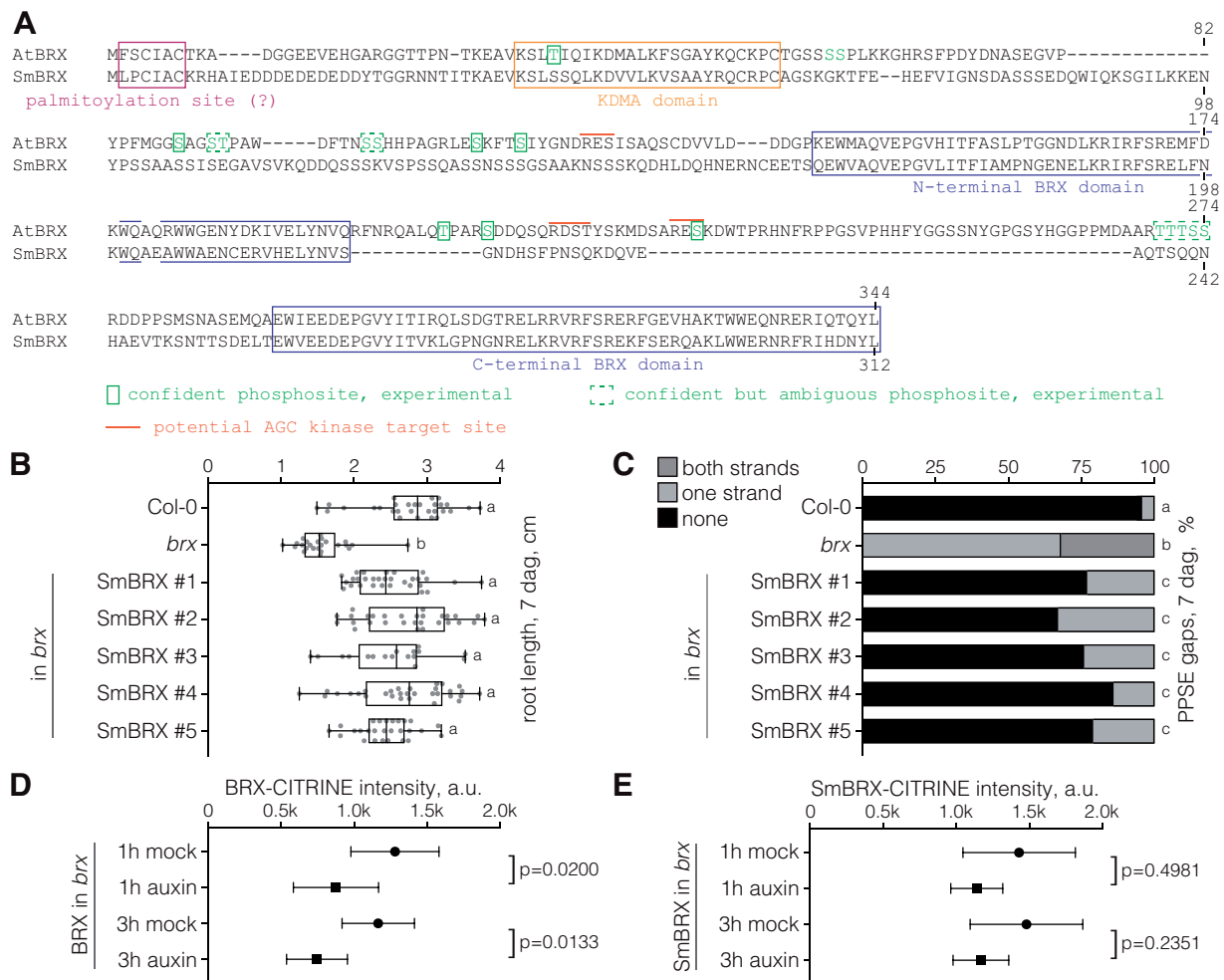


Figure 9 Partial rescue of the *brx* phenotype by a *S. moellendorffii* BRX homolog. **A**, Amino acid sequence alignment of *A. thaliana* (AtBRX) and *S. moellendorffii* (SmBRX) BRX protein homologs, highlighting key features. **B**, Root length of Col-0, *brx*, and transgenic lines expressing *A. thaliana* codon-optimized SmBRX-CITRINE fusion protein (five representative independent lines, $n = 17$ –31 roots). Box plots display second and third quartiles and the median, bars indicate maximum and minimum. Statistical significance was determined by ordinary one-way ANOVA. **C**, PPSE strand defects in the roots of the indicated genotypes, corresponding to (B) ($n = 34$ –106 roots). Statistical significance was determined by Fisher's exact test. **D** and **E**, Quantification of the indicated CITRINE fusion protein signal intensity at the rootward plasma membrane of developing PPSEs, 1 or 3 h after mock or auxin treatment ($n = 10$ –16 roots, average of 12–15 cells per root). Plot circles and squares display the mean, error bars indicate standard deviation. Statistical significance was determined by ordinary one-way ANOVA. Statistically significant different groups are indicated by different lowercase letters.

arrangement is the hallmark of BRX family proteins, and although single BRX domains are found in other proteins (Briggs et al., 2006; Furutani et al., 2020), their homology does not extend into the linker. Moreover, compared to the highly conserved BRX domains, the linker region is variable both in sequence and size. Because BRX family proteins are exchangeable in the context of stomata development (Rowe et al., 2019), but not in the context of root protophloem development (Briggs et al., 2006; Beuchat et al., 2010; Marhava et al., 2020), the linker region has apparently evolved to widen the developmental spectrum of BRX family protein functions. Indeed, the SmBRX protein is the smallest of the BRX homologs we could identify (One Thousand Plant Transcriptomes, 2019) because of its very short linker domain. It will be interesting to determine whether the evolution of the linker sequence correlates with the evolution of

PPSEs. Comprehensive testing of BRX homologs from various plant lineages for their functionality in *A. thaliana* could help to answer this question.

Materials and methods

Plant material and growth conditions

The *A. thaliana* accession Columbia-0 (Col-0) was the wild-type background for all lines used or produced in this study. Transgenes were assayed in the Col-0 or *brx-2* mutant (Rodrigues et al., 2009) background. The *brx brx1 brx2 brx3* quadruple mutant has been described before (Briggs et al., 2006; Rowe et al., 2019). The two independent AT2G21030 mutant alleles were created in Col-0 via CRISPR/Cas9 gene editing as described (Fauser et al., 2014; Graeff et al., 2020), using guide RNA 5'-GCC GAG AGA UGU ACA

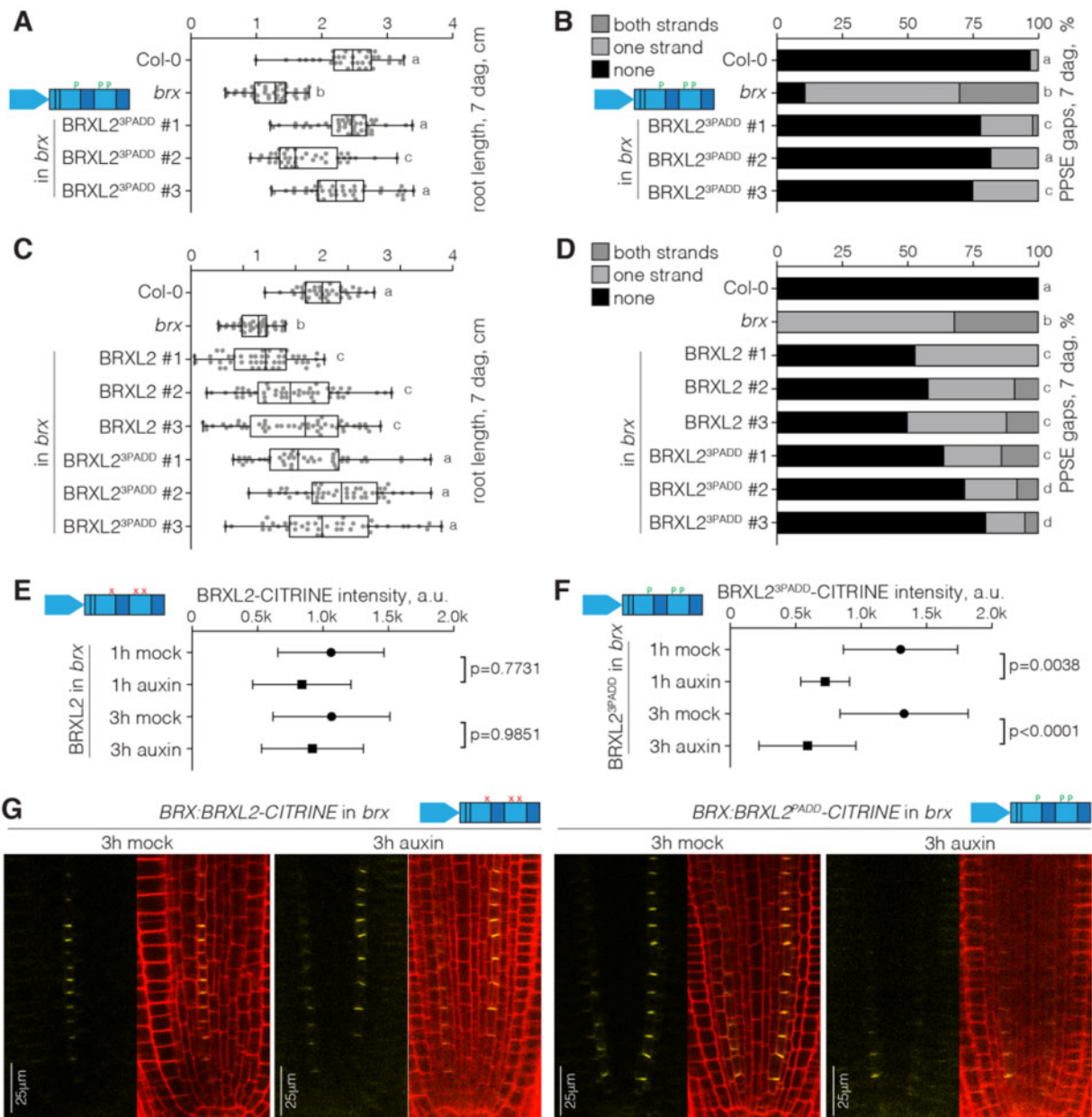


Figure 10 Engineering of PAX phosphosites renders BRXL2 auxin-responsive. A, Root length of Col-0, *brx*, and transgenic lines expressing a modified BRXL2^{3PADD}-CITRINE fusion protein (three representative independent lines, *n* = 33–44 roots). BRXL2^{3PADD} carries nine amino acid substitutions that introduce PAX target phosphosites (see Supplemental Figure S7). Box plots display second and third quartiles and the median, bars indicate maximum and minimum. Statistical significance was determined by ordinary one-way ANOVA. B, PPSE strand defects in the roots of the indicated genotypes, corresponding to (A) (*n* = 33–44 roots). Statistical significance was determined by Fisher's exact test. C, Root length of Col-0, *brx*, and transgenic lines expressing either BRXL2-CITRINE or the modified BRXL2^{3PADD}-CITRINE fusion protein (three "best" independent lines each, scored in parallel, *n* = 39–48 roots). Box plots display second and third quartiles and the median, bars indicate maximum and minimum. Statistical significance was determined by ordinary one-way ANOVA. D, PPSE strand defects in the roots of the indicated genotypes, corresponding to (C) (*n* = 39–48 roots). Statistical significance was determined by Fisher's exact test. E and F, Quantification of the indicated CITRINE fusion protein signal intensity at the rootward plasma membrane of developing PPSEs, 1 or 3 h after mock or auxin treatment (*n* = 15–30 roots, average of 12–15 cells per root). Plot circles and squares display the mean, error bars indicate standard deviation. Statistical significance was determined by ordinary one-way ANOVA. G, Confocal microscopy images of BRXL2-CITRINE or BRXL2^{3PADD}-CITRINE fusion protein expressed under the control of the BRX promoter in the *brx* mutant background (yellow fluorescence, left), illustrating auxin-induced plasma membrane dissociation of BRXL2^{3PADD}-CITRINE. (Right) overlay with PI cell wall staining (red fluorescence). Statistically significant different groups are indicated by different lowercase letters.

AUA AG-3'. For phenotyping assays, seeds were surface sterilized and then stratified for 2 days in the dark at $\sim 4^{\circ}\text{C}$ before germination and growth in continuous white light of $\sim 140\ \mu\text{E}$ intensity at $\sim 22^{\circ}\text{C}$ on vertically placed Petri dishes that contained $0.5 \times$ Murashige and Skoog (MS) medium supplemented with 1% agar and 0.3% sucrose.

Generation of transgenic lines

Transgenic constructs for plant transformation were created in suitable binary vectors and produced using standard molecular biology procedures and/or the GatewayTM cloning technology. The translational *BRX:BRX-CITRINE* and *BRX:BRXL2-CITRINE* fusions have been described before (Rodriguez-Villalon et al., 2014; Marhava et al., 2020). Similar constructs were created with *BRX* (AT1G31880) or *BRXL2* (AT3G14000) variants and *SmBRX* (SELMODRAFT_229072), all of which was obtained by gene synthesis (GeneArtTM) (Supplemental File S1). *SmBRX* was *A. thaliana* codon-optimized. The *CASP1* promoter has been previously described (Roppolo et al., 2011). For the genomic *BRXL1* (AT2G35600) and *BRXL2* constructs, the *BRXL1* promoter (4,061 bp upstream of the start codon) and *BRXL2* promoter (2,616 bp upstream of the start codon) were amplified and cloned into pDONR P4P1R. Genomic fragments of the *BRXL1* and *BRXL2* transcript regions without the stop codons were amplified and cloned from genomic DNA template. Partial *BRX* fragments were amplified with suitable oligonucleotides (Supplemental Table S1) and cloned using standard procedures. *BRX-BRXL2* hybrids were obtained by gene synthesis (GeneArtTM) (Supplemental File S1). Genes were cloned into pDONR 221. These entry clones were combined together with *CITRINE* in pDONR P2RP3 into the destination vector pH7m34GW by the multisite Gateway recombination system. For the AT2G21030 promoter, the 551 bp upstream of the ATG codon were cloned in front of an NLS-3XVENUS reporter gene as described (Marhava et al., 2018). The binary constructs were introduced into *Agrobacterium tumefaciens* strain GV3101pMP90 and transformed using the floral dip method.

Phenotyping

For root length measurements, plates were scanned and seedling root length was determined using Fiji software. For quantification of gap cells, root PPSEs were checked and counted by confocal microscopy (see below). Typically, 20–40 (length) and 15–20 (gap cells) roots were investigated for each genotype and/or treatment.

Auxin treatments

Five- to six-day-old seedlings were transferred onto liquid MS medium with or without $10\ \mu\text{M}$ 1-naphthyl-acetic acid pre-dissolved in dimethyl sulfoxide (DMSO) and kept in continuous white light of $\sim 140\ \mu\text{E}$ intensity at $\sim 22^{\circ}\text{C}$. Seedlings were removed for analysis at the indicated timepoints.

Confocal imaging and image analysis

For confocal microscopy images, a Zeiss LSM 700 confocal scanning microscope was used with the following fluorescence excitation–emission settings to visualize reporter genes and staining signals: *CITRINE* excitation 514 nm, emission 529 nm; *VENUS* excitation 515 nm, emission 528 nm; propidium iodide (PI) excitation 536 nm, emission 617 nm. Pictures were taken with $20\times$ or $40\times$ water/oil immersion objectives. Samples within one experiment were imaged with identical settings. For image analyses, ImageJ and Zeiss Zen 2011 (black edition) image analysis software were used. For signal quantifications (raw intensity without background correction), regions of interest were analyzed at the plasma membrane of developing PPSEs (typically 10–16 PPSEs per time point and treatment) in the same area of the root meristem. The average signal intensity per transgenic line was calculated as the mean of means (typically 12–20 roots per time point and treatment).

VISUAL assay and phosphoproteomics

The VISUAL assay was performed with *BRX:BRX-CITRINE* expressed in *brx* as described (Kondo et al., 2016; Marhava et al., 2018). Immuno-precipitated *BRX-CITRINE* samples were run on sodium dodecyl (lauryl) sulfate-polyacrylamide gel electrophoresis, and bands covering the *BRX-CITRINE* size range were cut out. Samples were prepared by semi-trypsin (two replicates) or semi-chymotrypsin (one replicate) digest for subsequent analysis by tandem mass spectrometry as described (Marhava et al., 2018).

In vitro kinase phosphorylation assays

Kinase assays with bacterially expressed D6PK, PAX, and *BRX-GST* fusion proteins were performed as described (Marhava et al., 2018). *BRX* point mutants were created by site-directed mutagenesis using standard procedures (Zourelidou et al., 2014).

Oocyte experiments

Auxin transport assays in *X. laevis* oocytes were performed as described (Marhava et al., 2018).

Quantification and statistical analysis

Statistical analyses were performed in Graphpad Prism software version 8.4.3. ANOVA and T-test results are provided in Supplemental File S2.

Sequence alignments

Sequence alignments were performed in SnapGene software version 5.1.3.

Accession numbers

Sequence data from this article can be found in the GenBank/EMBL libraries under the following accession numbers: *BRX* (AT1G31880), *BRXL1* (AT2G35600), *BRXL2* (AT3G14000), AT2G21030, and *SmBRX* (SELMODRAFT_229072).

Acknowledgments

We would like to thank Prof. Thomas Berleth for helpful comments on the manuscript, and Ms. Amelia Amiguet-Vercher and Ms. Floriana Misceo for technical assistance.

Funding

This work was funded by Swiss National Science Foundation grant 310030B_185379 (awarded to C.S.H.), and by the Deutsche Forschungsgemeinschaft SCHW751/12-2 (awarded to C.S.) and HA3468/6-1 (awarded to U.Z.H.).

Conflict of interest statement. None declared.

Supplemental data

The following materials are available in the online version of this article.

Supplemental Figure S1. Amino acid sequence alignment of *A. thaliana* BRX family proteins.

Supplemental Figure S2. Limited redundancy between BRX family genes in the root protophloem.

Supplemental Figure S3. Amino acid sequence alignment illustrating amino acid substitutions or additions to test putative functional features of BRX protein.

Supplemental Figure S4. Robust plasma membrane association of BRX variants.

Supplemental Figure S5. Ectopic expression of BRX–CITRINE fusion protein rescues the *brx* mutant.

Supplemental Figure S6. Schematic overview of the BRX–BRXL2 hybrid proteins tested in this study.

Supplemental Figure S7. Amino acid sequence alignment illustrating amino acid substitutions or additions to test the impact of putative D6PK/PAX target phosphosites on BRX and BRXL2 function in the root protophloem.

Supplemental Figure S8. Impact of amino acid substitutions in D6PK/PAX target phosphosites.

Supplemental Table S1. Primers used for genotyping and cloning.

Supplemental File S1. Sequences of BRX and BRXL2 hybrids and variants, and *A. thaliana*-codon-optimized *SmBRX*, obtained by site-directed mutagenesis or by gene synthesis.

Supplemental File S2. ANOVA and T-test results.

References

- Anne P, Hardtke CS (2017) Phloem function and development-biophysics meets genetics. *Curr Opin Plant Biol* **43**: 22–28
- Banks JA, Nishiyama T, Hasebe M, Bowman JL, Gribskov M, dePamphilis C, Albert VA, Aono N, Aoyama T, Ambrose BA et al. (2011) The Selaginella genome identifies genetic changes associated with the evolution of vascular plants. *Science* **332**: 960–963
- Barbosa ICR, Hammes UZ, Schwechheimer C (2018) Activation and polarity control of PIN-FORMED auxin transporters by phosphorylation. *Trends Plant Sci* **23**: 523–538
- Bauby H, Divol F, Truernit E, Grandjean O, Palauqui JC (2007) Protophloem differentiation in early *Arabidopsis thaliana* development. *Plant Cell Physiol* **48**: 97–109
- Beuchat J, Li S, Ragni L, Shindo C, Kohn MH, Hardtke CS (2010) A hyperactive quantitative trait locus allele of *Arabidopsis* BRX contributes to natural variation in root growth vigor. *Proc Natl Acad Sci USA* **107**: 8475–8480
- Bologna G, Yvon C, Duvaud S, Veuthey AL (2004) N-Terminal myristoylation predictions by ensembles of neural networks. *Proteomics* **4**: 1626–1632
- Breda AS, Hazak O, Hardtke CS (2017) Phosphosite charge rather than shootward localization determines OCTOPUS activity in root protophloem. *Proc Natl Acad Sci USA* **114**: 201703258
- Briggs GC, Mouchel CF, Hardtke CS (2006) Characterization of the plant-specific BREVIS RADIX gene family reveals limited genetic redundancy despite high sequence conservation. *Plant Physiol* **140**: 1306–1316
- Bringmann M, Bergmann DC (2017) Tissue-wide mechanical forces influence the polarity of stomatal stem cells in *Arabidopsis*. *Curr Biol* **27**: 877–883
- Cattaneo P, Graeff M, Marhava P, Hardtke CS (2019) Conditional effects of the epigenetic regulator JUMONJI 14 in *Arabidopsis* root growth. *Development* **146**: dev183905
- Dettmer J, Ursache R, Campilho A, Miyashima S, Belevich I, O'Regan S, Mullendore DL, Yadav SR, Lanz C, Beverina L, et al. (2014) CHOLINE TRANSPORTER-LIKE1 is required for sieve plate development to mediate long-distance cell-to-cell communication. *Nat Commun* **5**: 4276
- Fausser F, Schiml S, Puchta H (2014) Both CRISPR/Cas-based nucleases and nickases can be used efficiently for genome engineering in *Arabidopsis thaliana*. *Plant J* **79**: 348–359
- Furuta KM, Yadav SR, Lehesranta S, Belevich I, Miyashima S, Heo JO, Vaten A, Lindgren O, De Rybel B, Van Isterdael G et al. (2014) Plant development. *Arabidopsis* NAC45/86 direct sieve element morphogenesis culminating in enucleation. *Science* **345**: 933–937
- Furutani M, Hirano Y, Nishimura T, Nakamura M, Taniguchi M, Suzuki K, Oshida R, Kondo C, Sun S, Kato K et al. (2020) Polar recruitment of RLD by LAZY1-like protein during gravity signaling in root branch angle control. *Nat Commun* **11**: 76
- Graeff M, Rana S, Marhava P, Moret B, Hardtke CS (2020) Local and systemic effects of brassinosteroid perception in developing phloem. *Curr Biol* **30**: 1626–1638 e1623
- Grieneisen VA, Xu J, Maree AF, Hogeweg P, Scheres B (2007) Auxin transport is sufficient to generate a maximum and gradient guiding root growth. *Nature* **449**: 1008–1013
- Huang F, Zago MK, Abas L, van Marion A, Galván-Ampudia CS, Offringa R (2010) Phosphorylation of conserved PIN motifs directs *Arabidopsis* PIN1 polarity and auxin transport. *Plant Cell* **22**: 1129–1142
- Knoblauch M, Knoblauch J, Mullendore DL, Savage JA, Babst BA, Beecher SD, Dodgen AC, Jensen KH, Holbrook NM (2016) Testing the Munch hypothesis of long distance phloem transport in plants. *Elife* **5**: e15341
- Kondo Y, Nurani AM, Saito C, Ichihashi Y, Saito M, Yamazaki K, Mitsuda N, Ohme-Takagi M, Fukuda H (2016) Vascular cell induction culture system using *Arabidopsis* leaves (VISUAL) reveals the sequential differentiation of sieve element-like cells. *Plant Cell* **28**: 1250–1262
- Lucas WJ, Groover A, Lichtenberger R, Furuta K, Yadav SR, Helariutta Y, He XQ, Fukuda H, Kang J, Brady SM, et al. (2013) The plant vascular system: evolution, development and functions. *J Integr Plant Biol* **55**: 294–388
- Marhava P, Bassukas AEL, Zourelidou M, Kolb M, Moret B, Fastner A, Schulze WX, Cattaneo P, Hammes UZ, Schwechheimer C, et al. (2018) A molecular rheostat adjusts auxin flux to promote root protophloem differentiation. *Nature* **558**: 297–300
- Marhava P, Aliaga Fandino AC, Koh SWH, Jelinkova A, Kolb M, Janacek DP, Breda AS, Cattaneo P, Hammes UZ, Petrasek J, et al. (2020) Plasma membrane domain patterning and self-reinforcing polarity in *Arabidopsis*. *Dev Cell* **52**: 223–235 e225

- Moret B, Marhava P, Aliaga Fandino AC, Hardtke CS, Ten Tusscher KHW** (2020) Local auxin competition explains fragmented differentiation patterns. *Nat Commun* **11**: 2965.
- Mouchel CF, Briggs GC, Hardtke CS** (2004) Natural genetic variation in *Arabidopsis* identifies BREVIS RADIX, a novel regulator of cell proliferation and elongation in the root. *Genes Dev* **18**: 700–714
- One Thousand Plant Transcriptomes Initiative** (2019) One thousand plant transcriptomes and the phylogenomics of green plants. *Nature* **574**: 679–685
- Rodriguez A, Santiago J, Rubio S, Saez A, Osmont KS, Gadea J, Hardtke CS, Rodriguez PL** (2009) The short-rooted phenotype of the brevis radix mutant partly reflects root abscisic acid hypersensitivity. *Plant Physiol* **149**: 1917–1928
- Rodriguez-Villalon A, Gujas B, Kang YH, Breda AS, Cattaneo P, Depuydt S, Hardtke CS** (2014) Molecular genetic framework for protophloem formation. *Proc Natl Acad Sci USA* **111**: 11551–11556
- Roppolo D, De Rybel B, Denervaud Tendon V, Pfister A, Alassimone J, Vermeer JE, Yamazaki M, Stierhof YD, Beeckman T, Geldner N** (2011) A novel protein family mediates Casparian strip formation in the endodermis. *Nature* **473**: 380–383
- Rowe MH, Dong J, Weimer AK, Bergmann DC** (2019) A plant-specific polarity module establishes cell fate asymmetry in the *Arabidopsis* stomatal lineage. *bioRxiv*. doi.org/10.1101/614636
- Sabatini S, Beis D, Wolkenfelt H, Murfett J, Guilfoyle T, Malamy J, Benfey P, Leyser O, Bechtold N, Weisbeek P, et al.** (1999) An auxin-dependent distal organizer of pattern and polarity in the *Arabidopsis* root. *Cell* **99**: 463–472
- Santuari L, Scacchi E, Rodriguez-Villalon A, Salinas P, Dohmann EM, Brunoud G, Vernoux T, Smith RS, Hardtke CS** (2011) Positional information by differential endocytosis splits auxin response to drive *Arabidopsis* root meristem growth. *Curr Biol* **21**: 1918–1923
- Scacchi E, Osmont KS, Beuchat J, Salinas P, Navarrete-Gomez M, Trigueros M, Ferrandiz C, Hardtke CS** (2009) Dynamic, auxin-responsive plasma membrane-to-nucleus movement of *Arabidopsis* BRX. *Development* **136**: 2059–2067
- Scacchi E, Salinas P, Gujas B, Santuari L, Krogan N, Ragni L, Berleth T, Hardtke CS** (2010) Spatio-temporal sequence of cross-regulatory events in root meristem growth. *Proc Natl Acad Sci USA* **107**: 22734–22739
- Sieburth LE, Meyerowitz EM** (1997) Molecular dissection of the AGAMOUS control region shows that cis elements for spatial regulation are located intragenically. *Plant Cell* **9**: 355–365
- Tan S, Zhang X, Kong W, Yang XL, Molnar G, Vondrakova Z, Filepova R, Petrasek J, Friml J, Xue HW** (2020) The lipid code-dependent phosphoswitch PDK1-D6PK activates PIN-mediated auxin efflux in *Arabidopsis*. *Nat Plants* **6**: 556–569
- Xiao Y, Offringa R** (2020) PDK1 regulates auxin transport and *Arabidopsis* vascular development through AGC1 kinase PAX. *Nat Plants* **6**: 544–555
- Zegzouti H, Li W, Lorenz TC, Xie M, Payne CT, Smith K, Glenny S, Payne GS, Christensen SK** (2006) Structural and functional insights into the regulation of *Arabidopsis* AGC VIIIa kinases. *J Biol Chem* **281**: 35520–35530
- Zourelidou M, Absmanner B, Weller B, Barbosa IC, Willige BC, Fastner A, Streit V, Port SA, Colcombet J, de la Fuente van Bentem S, et al.** (2014) Auxin efflux by PIN-FORMED proteins is activated by two different protein kinases, D6 PROTEIN KINASE and PINOID. *Elife* **3**: e02860